

First Detection of 350 Micron Polarization From a Radio-loud AGN

Sang-Sung Lee^{1,2}, Sincheol Kang^{1,2}, Do-Young Byun¹, Nicholas Chapman³, Giles Novak³, Sascha Trippe⁴, Juan Carlos Algaba¹, and Motoki Kino¹

ABSTRACT

We report the first detection of linearly polarized emission at an observing wavelength of 350 μm from the radio-loud Active Galactic Nucleus 3C 279. We conducted polarization observations for 3C 279 using the SHARP polarimeter in the Caltech Submillimeter Observatory on 2014 March 13 and 14. For the first time, we detected the linear polarization with the degree of polarization of $13.3\% \pm 3.4\%$ (3.9σ) and the Electric Vector Position Angle (EVPA) of $34.7^\circ \pm 5.6^\circ$. We also observed 3C 279 simultaneously at 13, 7, and 3.5 mm in dual polarization with the Korean very long baseline interferometry (VLBI) Network on 2014 March 6 (single dish) and imaged in milliarcsecond (mas) scales at 13, 7, 3.5, and 2.3 mm on March 22 (VLBI). We found that the degree of linear polarization increases from 10% to 13% at 13 mm to 350 μm and the EVPAs at all observing frequencies are parallel within $< 10^\circ$ to the direction of the jet at mas scale, implying that the integrated magnetic fields are perpendicular to the jet in the innermost regions. We also found that the Faraday rotation measures RM are in a range of $-6.5 \times 10^2 \sim -2.7 \times 10^3 \text{ rad m}^{-2}$ between 13 and 3.5 mm, and are scaled as a function of wavelength: $|\text{RM}| \propto \lambda^{-2.2}$. These results indicate that the mm and sub-mm polarization emission are generated in the compact jet within 1 mas scale and affected by a Faraday screen in or in the close proximity of the jet.

Subject headings: polarization — radiation mechanisms: non-thermal — techniques: polarimetric — galaxies: active — galaxies: jets — quasars: individual (3C 279)

1. Introduction

Radio-loud active galactic nuclei (AGNs) are known to generate highly collimated relativistic jets. Polarimetric observations at millimeter wavelengths of the radio-loud AGNs find polarized synchrotron emission with the degree of linear polarization in the range of 1%–19% with a mean value

of 4% (Trippe et al. 2010; Agudo et al. 2010). Polarization observations enable us to understand geometrical structure and intensity of magnetic fields, particle densities and structures of emission region (e.g., Saikia & Salter 1988, and references therein).

Synchrotron emission at millimeter (mm) and sub-millimeter (sub-mm) wavelengths comes from the innermost compact regions of the relativistic jet, most likely from within the most upstream emission region in the compact radio jet (the core) in Very Long Baseline Interferometry (VLBI) observations (e.g., Lee et al. 2008; Jorstad et al. 2007). The mm and sub-mm emission is typically optically thin and less affected by Faraday rotation than at longer wavelengths (see e.g., Agudo et al. 2010). Since the amount of Faraday rotation (RM) is proportional to the squares of observing wave-

¹Korea Astronomy and Space Science Institute, Daedeokdae-ro 776, Yuseong-gu, Daejeon 305-348, Korea; sslee@kasi.re.kr

²Korea University of Science and Technology, 176 Gajeong-dong, Yuseong-gu, Daejeon 305-350, Korea

³Center for Interdisciplinary Exploration and Research in Astrophysics (CIERA) and Department of Physics & Astronomy, Northwestern University, 2145 Sheridan Road, Evanston, IL 60208, USA

⁴Department of Physics and Astronomy, Seoul National University, 599 Gwanak-ro, Gwanak-gu, Seoul 151-742, Republic of Korea

length (λ) as $\chi_{\text{obs}} = \chi_{\text{int}} + \text{RM}\lambda^2$ (where RM^1 is the Faraday rotation measure, χ_{obs} is the observed electric vector linear polarization angle of a source, and χ_{int} is the intrinsic polarization angle), mm and sub-mm polarization observations may experience much less Faraday rotation than centimeter wavelength observations. Provided that the Faraday rotation measure is constant, at $\lambda 350 \mu\text{m}$, a rotation measure of $1.4 \times 10^5 \text{ rad m}^{-2}$ causes a rotation of the Electric Vector Position Angle (EVPA) by 1° , whereas it causes rotation by 3200° at 2 cm. Accordingly, such high rotation measures are studied best at (sub)mm wavelengths where $\chi_{\text{obs}} = \chi_{\text{obs}} \pm n\pi$ ambiguities can be avoided. This indicates that the mm and sub-mm observations may be much more efficient to investigate the intrinsic linear polarization properties of the relativistic jets than centimeter radio observations.

Previous mm/sub-mm polarization observations include several polarimetric mm surveys of AGNs with the IRAM Plateau de Bure Interferometer (Trippé et al. 2010) and the IRAM 30 m telescope (Agudo et al. 2010, 2014), and polarimetric studies of individual AGNs (Stevens et al. 1996; Jorstad et al. 2005, 2007; Trippé et al. 2012a,b; Plambeck et al. 2014; Martí-Vidal et al. 2015). These studies report that degree of linear polarization p of the radio loud AGNs is in the range of 1%-19% at mm/sub-mm wavelengths.

Among the radio loud AGNs in these studies, 3C 279 (1253-055, $z = 0.538$) is one of the brightest, highly polarized AGNs. In 2010 August, as reported by Agudo et al. (2014), the degree of linear polarizations of 3C 279 was $3.9\% \pm 0.3\%$ at 3.5 mm and of $< 6.6\%$ at 1.3 mm. The EVPA was measured only at 3.5 mm to be $107^\circ \pm 1.8^\circ$. Stevens et al. (1996) showed that 3C 279 was highly polarized with $p = 10.4\% \pm 0.6\%$ and $p = 13.5\% \pm 1.4\%$ at 1.1 and 0.8 mm. The flux densities of 3C 279 were $7.6 \pm 0.5 \text{ Jy}$ and $5.3 \pm 0.4 \text{ Jy}$ at each wavelengths on 1995 August 2. The polarization position angle of 76° at both 1.1 and 0.8 mm implies that the magnetic field is aligned orthogonal to the centimeter VLBI jet to within about 6° . Jorstad et al. (2007) also reported that 3C 279 was the most highly polarized AGNs among their

sources with $p = 3\% - 9\%$ at 1.3 mm in 1998-1998 and $p = 7\% - 11\%$ at 0.8 mm in 2000-2001, and with the mean polarization position angle 67° at 1.3 mm and 65° at 0.8 mm. These results clearly show that mm/sub-mm polarization of 3C 279 is significantly variable.

In order to investigate intrinsic linear polarization properties of the relativistic jet of 3C 279, we conducted (quasi-)simultaneous multiwavelength polarization observations at 1.3 cm, 7 mm, 3.5 mm, and $350 \mu\text{m}$. In this letter, we present results of mm and sub-mm observations of 3C 279 using the Korean VLBI Network (KVN) and the Caltech Submillimeter Observatory (CSO), which yielded the first detection of linearly polarized emission of 3C 279 at an observing wavelength of $350 \mu\text{m}$. Combining the KVN and CSO polarization observations, we aim to study the magnetic field properties in the innermost regions of the jet and their environments. Throughout this letter, we assume a cosmology with $H_0 = 70 \text{ km s}^{-1} \text{ Mpc}^{-1}$, $\Omega_M = 0.3$, and $\Omega_\lambda = 0.7$.

2. Observations and data reduction

We conducted polarimetric observations of 3C 279 on 2014 March 13 and 14 UT using the SHARP polarimeter at the CSO. SHARP is a fore-optics module that adds polarimetric capability to SHARC-II, a 12×32 pixel bolometer array used at the CSO (Dowell et al. 2003; Li et al. 2008). The wavelength of the observations was $350 \mu\text{m}$. We observed 3C 279 for 30 half-wave plate (HWP) cycles, where one HWP cycle consists of the observations of the source at four HWP angles and takes about 7 minutes. The chop throw was $3'$ or $5'$ and the optical depth at $350 \mu\text{m}$ ranged from 0.90 to 2.6 (or 0.05-0.1 at 225 GHz). Details about SHARP and data reduction procedures can be found in Davidson et al. (2011) and Chapman et al. (2013). Following these procedures, we created maps of Stokes I (total intensity) and Stokes Q and U (linear polarization).

We also conducted single dish simultaneous multifrequency (22, 43, and 86 GHz) polarimetric observations of 3C 279 using 21 m radio telescopes of KVN on 2014 March 6, and conducted high resolution simultaneous multifrequency (22, 43, 86, and 129 GHz) VLBI observations of the source on 2014 March 22. KVN is a mm-dedicated

¹ RM in the observer's frame can be scaled by a factor of $(1+z)^2$ in the rest frame. In this letter, we present RM in the observer's frame.

VLBI network consisting of three 21 m radio telescopes in Korea with the maximum baseline of 476 km (Lee et al. 2011, 2014).

A polarimetric observation of the source consists of on-off switching observations with the on-source integration time of ~ 6 minutes. Cross-scan pointing and antenna gain calibration measurements were conducted before every polarimetric observation. We observed planets for calibrating instrumental polarization, and Crab nebula as a polarization angle calibrator. The phase difference between left and right circularly polarized signals is derived from the complex cross-power spectra measured with the KVN digital spectrometer. The complex cross-power spectra are corrected for instrumental polarization using those of planets. The phase of the cross-power spectra are corrected for a phase rotation due to parallactic angle change and then used to estimate the polarization angle. The estimated polarization angle is corrected by $\chi = 154^\circ$ at 22 GHz, 43 GHz, and 86 GHz bands, which is the intrinsic χ of Crab nebula (Wright & Forster 1980; Flett & Henderson 1979; Aumont et al. 2010). The rms uncertainties of the linear polarization observations are about 10 mJy and 15 mJy at 22 GHz and 43 GHz, respectively. The systematic error of the polarization angle measurements is 2° at both frequencies. The typical instrumental polarization leakage of the KVN system is $< 5\%$ at both frequencies. Details about the data reduction pipeline for the polarimetric observations and the polarimetric capability of the KVN will be described elsewhere (Byun, D.-Y. et al. 2015, in preparation).

The VLBI observations of the source were conducted as part of the iMOGABA project (Lee et al. 2013). The source was observed with 3 scans of 5 minutes long each during UT 12:30:00 – 15:05:00. The observing frequency band was 22.700–22.764 GHz, 43.400–43.464 GHz, 86.800–86.864 GHz, 129.300–129.364 GHz in left-hand circular polarization. We conducted sky tipping curve measurements every hour in order to trace changes in the opacity of the atmosphere during the observations. The data were digitized in 2-bit sampling mode, and the digitized signals were processed by the digital filter bank to be 16 sub-bands of 16 MHz and divided evenly for four frequency bands. The Mark 5B system at a recording rate of 1024 Mbps was used for recording the data. The correlation

of the recorded data was done with the DiFX software correlator. We followed the standard data reduction procedure for the KVN observations as described in Lee et al. (2014), and obtained the high resolution VLBI images for the source.

The 1 mm (2014 March 7) and 850 μm (2014 March 20) flux density data were obtained at the Submillimeter Array (SMA), an eight-element interferometer located near the summit of Mauna Kea (Hawaii). 3C 279 is included in an ongoing monitoring program at the SMA to determine the flux densities of compact extragalactic radio sources that can be used as calibrators at mm and sub-mm wavelengths (Gurwell et al. 2007). Observations of calibrators were conducted every 3-5 minutes, and the measured source signal strength calibrated against known standards, typically solar system objects (Titan, Uranus, Neptune, or Callisto). Data from this program are updated regularly and are available at the SMA website (<http://sma1.sma.hawaii.edu/callist/callist.html>).

Optical (5000-7000 \AA) spectropolarimetric data was obtained at the Steward Observatory, as part of a monitoring program of gamma-ray blazars. The data used in this paper is taken on 2014 March 25. The detailed procedure of data analysis is described in Smith (2009).

3. Results

Our final map at 350 μm (Figure 1) obtained using the SHARP has a resolution of $10''$. Because 3C 279 is a point source at our resolution, we only extracted a polarization vector at the position of the peak flux. Degree of polarization cannot be negative, which leads to a small positive bias, for which we corrected (Hildebrand et al. 2000). After debiasing, the degree of linear polarization p is $13.3\% \pm 3.4\%$ (3.9σ), and the polarization angle χ is $34.7^\circ \pm 5.6^\circ$ measured east of north. This is the first detection of linearly polarized emission at the observing wavelength of 350 μm from AGNs. The polarization observations using the KVN telescopes at mm wavelengths, 13 mm, 7 mm, and 3.5 mm, have been processed with the KVN pipeline, and resulted in the degree of linear polarization $p = 10\% - 12\%$ and the polarization angle $\chi = 32^\circ - 41^\circ$. From the optical spectropolarimetric observations, we found that the optical polarization degree is $12.35\% \pm 0.05\%$ and the polarization angle

TABLE 1
RESULTS OF THE POLARIZATION OBSERVATIONS

Epoch (1)	Telescope (2)	λ (mm) (3)	ν (GHz) (4)	p (%) (5)	σ_p (%) (6)	χ (deg) (7)	σ_χ (deg) (8)	S_ν (Jy) (9)
2014 Mar 6	KVN	13	22.4	10.0	0.1	31.0	0.8	33.4 ± 0.3
		7.0	43.1	10.5	0.2	35.8	1.3	25.6 ± 0.5
		3.5	86.2	11.6	0.2	41.5	0.9	18.8 ± 0.5
2014 Mar 13 and 14	CSO	0.35	860	13.3	3.4	34.7	5.6	...
2014 Mar 25	Steward	5000-7000Å	...	12.4	0.04	40.5	0.1	...

NOTE.—Column designation: (1) - observation epoch; (2) - telescope; (3) - observing wavelength in mm; (4) - observing frequency in GHz; (5) - degree of linear polarization; (6) - standard deviation of the degree of linear polarization; (7) - Electric Vector Position Angle (EVPA) in degree; (8) - standard deviation of the EVPA; (9) - flux density in Jansky.

TABLE 2
IMAGE PARAMETERS

λ (1)	$B_{\text{maj}}:B_{\text{min}}:B_{\text{PA}}$ (2)	S_{CLEAN} (3)	S_p (4)	σ (5)	Comp (6)	S_{tot} (7)	S_{peak} (8)	d (9)	r (10)	θ (11)	r' (12)	θ' (13)
13 mm	5.88:3.56:-70.2	26.6	25.4	53.7	C1	15.7 ± 1.9	15.8 ± 1.4	0.23 ± 0.03	0.37 ± 0.02	63.3 ± 2.5	0.00	0.0
					C2a	10.2 ± 1.5	10.3 ± 1.1	0.23 ± 0.05	0.59 ± 0.02	-117.2 ± 2.3	0.96	-117.0
					J2	0.295 ± 0.149	0.288 ± 0.104	1.80 ± 0.65	6.73 ± 0.33	-140.5 ± 2.8	7.07	-139.3
					J3	0.258 ± 0.165	0.265 ± 0.118	2.02 ± 0.90	17.23 ± 0.45	-138.5 ± 1.5	17.57	-138.1
7 mm	2.90:1.79:-70.4	19.6	17.2	38.6	C1	11.7 ± 0.1	11.0 ± 0.1	0.58 ± 0.00	0.29 ± 0.00	43.4 ± 0.4	0.00	0.0
					C2b	7.65 ± 0.1	7.64 ± 0.07	0.08 ± 0.00	0.48 ± 0.00	-133.4 ± 0.0	0.77	-134.6
					J1	0.624 ± 0.053	0.556 ± 0.035	0.78 ± 0.05	3.33 ± 0.02	-146.3 ± 0.4	3.62	-145.5
3.5 mm	1.62:0.81:-66.1	13.4	7.57	92.7	C1	6.00 ± 0.12	5.73 ± 0.08	0.24 ± 0.00	0.37 ± 0.00	30.1 ± 0.3	0.00	0.0
					C2b	6.36 ± 0.16	5.81 ± 0.11	0.33 ± 0.01	0.35 ± 0.00	-148.4 ± 0.5	0.72	-149.2
					J1	1.52 ± 0.68	0.52 ± 0.22	1.18 ± 0.50	2.98 ± 0.25	-147.7 ± 4.7	3.35	-147.9
2.3 mm	1.03:0.58:-52.2	7.74	3.35	44.0	C1	3.91 ± 0.29	3.35 ± 0.19	0.30 ± 0.02	0.06 ± 0.01	-79.4 ± 8.3	0.00	0.0
					C2b	1.87 ± 0.16	1.87 ± 0.12	0.04 ± 0.00	0.81 ± 0.00	-146.3 ± 0.1	0.79	-150.3
					J1a	0.988 ± 0.10	0.99 ± 0.07	0.03 ± 0.00	1.76 ± 0.00	-143.5 ± 0.1	1.73	-145.3
					J1b	1.34 ± 0.20	1.11 ± 0.13	0.35 ± 0.04	2.35 ± 0.02	-148.0 ± 0.5	2.33	-149.4
					J2a	0.483 ± 0.11	0.49 ± 0.08	0.06 ± 0.02	4.56 ± 0.01	-145.5 ± 0.1	4.54	-146.2
					J2b	0.544 ± 0.06	0.48 ± 0.04	0.27 ± 0.02	5.32 ± 0.01	-145.4 ± 0.1	5.30	-146.0

NOTE.—Column designation: (1) - Observing wavelength; (2) - restoring beam-major axis (mas): minor axis (mas): position angle of the major axis ($^\circ$); (3) - total CLEAN flux density (Jy); (4) - peak flux density in the image (Jy beam^{-1}); (5) - off-source RMS in the image (mJy beam^{-1}); (6) - Gaussian jet components; (7) - model flux density of the component (Jy); (8) - peak brightness of individual component measured in the image (mJy beam^{-1}); (9) - size (mas); (10) - radius (mas); (11) - position angle ($^\circ$); (12) - radius with respect to the C1 component (mas); (13) - position angle with respect to the C1 component ($^\circ$).

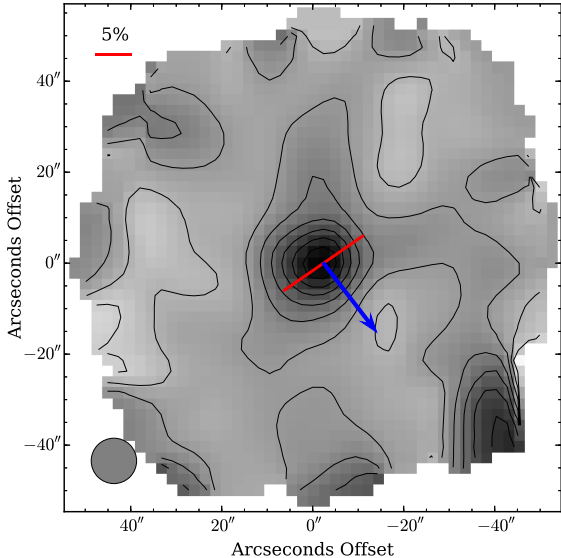


Fig. 1.— Polarization map of 3C 279. Contours show the $350\ \mu\text{m}$ intensity (Stokes I), ranging from 20% of the peak flux, in steps of 10%. The red vector shows the measured $350\ \mu\text{m}$ polarization at the peak, where the angle of the vector has been rotated by 90° to show the inferred magnetic field direction. The length of the vector is proportional to the degree of polarization. The gray circle at the bottom denotes the SHARP beam size, $10''$. The large blue arrow shows the mean position angle (-142.2°) of the jets observed at 22-129 GHz using KVN.

is $\chi = 40.5^\circ \pm 0.1^\circ$. We summarized the results of the polarization observations in Table 1.

From the mm and sub-mm polarization observations, we found that the degree of linear polarization increases from 10% to 13% as the observing wavelength becomes shorter and the polarization angle rotates from 30° to 41° to east from north and at $350\ \mu\text{m}$ the angle rotates back to 35° , as shown in Figures 2a and 2b. With the polarization angles observed at multiwavelengths, we estimated RM of $-647 \pm 206\ \text{rad m}^{-2}$ between 7-13 mm, $-2713 \pm 766\ \text{rad m}^{-2}$ between 3.5-7 mm and $-1022 \pm 264\ \text{rad m}^{-2}$ between 3.5 and 13 mm. By assuming that the polarized emission at radio to optical are coming from a very compact region (or the same region), we may be able to estimate the RM of $-1005 \pm 117\ \text{rad m}^{-2}$.

The flux densities at 13-3.5 mm were > 18 Jy with a spectral index of $\alpha = -0.42 \pm 0.01$ ($S_\nu \propto \nu^\alpha$). The flux densities obtained with SMA are 9.9 ± 0.5 Jy at 1 mm on 2014 March 7, and 7.9 ± 0.4 Jy at $850\ \mu\text{m}$ on 2014 March 20, yielding a spectral index of $\alpha = -0.64 \pm 0.02$. This implies that 3C 279 is a flat spectrum source at cm and mm wavelengths, and its spectrum becomes steeper at mm and sub-mm wavelengths as shown in Figure 2c. We obtained the *Planck* flux density of 3C 279 from the recently released *Planck* Collaboration (2013) catalog, which yielded comparable spectral indices of -0.25 ± 0.04 and -0.63 ± 0.01 at the frequency ranges of 44-100 and 100-857 GHz, respectively, with those obtained from KVN and SMA observations. We found that the spectrum of the source becomes steeper at >100 GHz. The difference of the flux densities at the similar frequencies between the KVN/SMA and the *PLANCK* spectra is mainly due to the source variability.

In Figure 3, we present CLEANed images for 3C 279 obtained with KVN observations simultaneously at 13, 7, 3.5, and 2.3 mm on 2014 March 22. Circular Gaussian models are fitted to the CLEANed images. The VLBI images at mm wavelengths show core-dominated structures within a few mas and faint jet components in south-west direction. More detailed parameters of the images are summarized in Table 2. The uncertainties of the parameters are estimated by following Lee et al. (2008). We found that two comparable jet components separated by <1 mas, i.e., the C1 and C2a(b) components, and they are the brightest jet components in the images at all wavelengths. All jet components are aligned in a mean position angle of -142.4° , taking into account the estimated jet position angle with respect to the C1 component. The direction of the jets is aligned to the polarization position angle at mm-to-optical within $< 10^\circ$. This implies that the dominant magnetic field direction is perpendicular to the direction of the mm jet at mas scales.

4. Discussion and Conclusions

High resolution VLBI observations of 3C 279 show that the combined flux density of the C1 and C2a(b) components contributes over 90% of the total CLEAN flux density at 13-3.5 mm, and

over 70% of that at 2.3 mm, implying that most of mm emission originate from very compact regions within <1 mas (<6.3 pc). Previous VLBI observations also confirmed the compact jet structures (e.g., Jorstad et al. 2005; Lee et al. 2008; Homan et al. 2009). In addition to the compactness of the source, our KVN VLBI observations at multifrequency revealed the spectral properties of the innermost regions, i.e., the components C1 and C2. As shown in Figure 2c, there is a break at 86 GHz on the CLEAN spectrum of the source, implying that the source becomes optically thin above the frequency on mas scales. The spectral break seems mainly due to the spectrum of the component C2 which shows very steep spectrum between 86 and 129 GHz. Therefore, we may expect that the component C1 dominates the sub-mm emission and hence the sub-mm (350 μ m) emission regions are located within the C1 component.

In order to further investigate the mm and sub-mm polarized emission predominantly originated in the components C1 and C2 (i.e., within <1 mas), the degree of linear polarization at 13 mm-350 μ m was fitted with a power law model, $p(\%) = A\lambda^\beta$, suggested by Tribble (1991) and modified by Farnes et al. (2014) for explaining external Faraday depolarization (see Burn 1966), where A is constant, β is a polarization spectral index, and λ is an observing wavelength in cm. A best fit power law to the data yielded $A = 10.3 \pm 0.08$ and $\beta = -0.11 \pm 0.01$ which implies that the effect of external Faraday depolarization is very small within the observing beams of KVN and CSO. We also expect that our measurements of the polarization with different angular resolutions (10''-130'') are not significantly affected by beam depolarization effect, since the predominantly polarized emission regions are compact enough to be covered by the resolutions. Therefore the best fit result seems to indicate that (a) any existing Faraday screen does not significantly affect the polarized emission of 3C 279 at mm and sub-mm, or (b) a Faraday screen contains a uniform field, even if there is a Faraday rotation by the Faraday screen (Farnes et al. 2014). In fact, the estimated $|\text{RM}|$ of 647-2713 rad m^{-2} over the wavelengths 3.5-13 mm may indicate that the polarized emission at the wavelengths is passing through a Faraday screen which may con-

tain a uniform field. However, due to the resolution limitation, the observations only probe the overall direction of the magnetic field in the mm emission-dominated region. Obviously, in the future, short-millimeter (and sub-millimeter) VLBI observations (Fish et al. 2013; Tilanus et al. 2014) are much awaited to really probe the geometry of the magnetic field in detail.

Jorstad et al. (2007) reported that RM at shorter wavelengths is larger in relativistic radio jet with a wavelength dependence of $\text{RM} : |\text{RM}(\lambda)| \propto \lambda^{-a}$, assuming that the Faraday rotation originates in or in close proximity of the jet. For optically thick VLBI cores, where the optical depth is unity, a simple jet model is assumed as the following (see also Lobanov 1998): the distance r of the emission region to the central engine depends on the observing wavelength λ as $r \propto \lambda$, the electron density n_e and the magnetic field parallel to the line of sight B_{\parallel} in the region scale geometrically as $n_e \propto r^{-2}$ (for the spherical or conical geometries of the jet) and $B_{\parallel} \propto r^{-1}$, and the path length l increases as a function of r as $l \propto r$. The RM dependence on the electron density, the parallel magnetic field strength, and the path length $\text{RM} \propto \int n_e B_{\parallel} dl$ gives $|\text{RM}(\lambda)| \propto \lambda^{-2}$. The authors found $a = 1.8 \pm 0.5$ for eight AGNs observed at centimeter to mm wavelengths. This wavelength dependence of RM was confirmed for 1418+546 with $a = 1.9 \pm 0.3$ (Trippe et al. 2012a), for 3C 84 with $a = 2$ (Farnes et al. 2014), and for PKS 1830-211 with $a \approx 2.4$ (Martí-Vidal et al. 2015), although a larger value of $a = 3.6 \pm 1.3$ was reported (Algaba 2013). For 3C 279, we found that the 7-13 mm $|\text{RM}|$ of 6.5×10^2 rad m^{-2} can be scaled by $\lambda^{-2.2}$ (i.e., $a = 2.2$) to get $|\text{RM}| \sim 2.7 \times 10^3$ rad m^{-2} at 3.5-7 mm, which is consistent with the measured value. This may imply that the Faraday rotation at mm wavelength originate in or in the close proximity of the jet whose geometry is spherical or conical. Caution should be taken here, as this model may not fully apply for the mm emission from 3C 279, since the presence of knots (e.g., shocks) such as C1 and C2 components, visible at mm wavelengths, may indicate that the innermost jet is composed of both smooth and knotty components (e.g., Kudryavtseva et al. 2011).

The first detection of 350 μ m polarized emission of 3C 279, the multiwavelength mm polarization

measurements, and the high resolution multiwavelength VLBI observations on mas scales enable us to find that the mm and sub-mm polarization emission of 3C 279 are generated in the compact jet regions within 1 mas scale and affected by a Faraday screen in or in the close proximity of the jet whose geometry is spherical or conical. We also found that the dominant magnetic field direction in the region is perpendicular to the direction of the mm jet at mas scale.

We thank the CSO staff for obtaining the 350 μ m data, and the KVN staff for operating the array and correlating the data. The KVN is a facility operated by the Korea Astronomy and Space Science Institute. The KVN operations are supported by Korea Research Environment Open NETwork which is managed and operated by Korea Institute of Science and Technology Information. We thank Mark Gurwell for providing the data obtained at the SMA, which is a joint project between the Smithsonian Astrophysical Observatory and the Academia Sinica Institute of Astronomy and Astrophysics and is funded by the Smithsonian Institution and the Academia Sinica. Data from the Steward Observatory spectropolarimetric monitoring project which is supported by Fermi Guest Investigator grants NNX08AW56G, NNX09AU10G, and NNX12AO93G, were used.

REFERENCES

- Agudo, I., Thum, C., Wiesemeyer, H., & Krichbaum, T. P. 2010, *ApJS*, 189, 1
- Agudo, I., Thum, U., Gómez, J. L., & Wiesemeyer, H. 2014, *A&A*, 566, 59
- Algaba, J. C. 2013, *MNRAS*, 429, 3551
- Aumont, J., Conversi, L., Thum, C., et al. 2010, *A&A*, 514, 70
- Burn, B. J. 1966, *MNRAS*, 133, 67
- Davidson, J. A., Novak, G., Matthews, T. G., et al. 2011, *ApJ*, 732, 97
- Chapman, N. L., Davidson, J. A. Goldsmith, P. F., et al. 2013, *ApJ*, 770, 151
- Farnes, J. S., O’Sullivan, S. P., Corrigan, M. E., & Gaensler, B. M. 2014, *ApJ*, 795, 63
- Dowell, C. D., Allen, C. A., Babu, R. S., et al. 2003, in *Proc. SPIE* 4855, 73
- Fish, V., Alef, W., Anderson, J., et al. 2013, *ArXiv e-prints*, 1309.3519
- Flett, A. M.; Henderson, C. 1979, *MNRAS*, 189, 867
- Gurwell, M. A., Peck, A. B., Hostler, S. R., Darrah, M. R., & Katz, C. A. 2007, *ASP Conf. Ser.* 375, *From Z-Machines to ALMA: (Sub)millimeter Spectroscopy of Galaxies*, ed. A. J. Baker, J. Glenn, A. I. Harris, J. G. Mangum, & M. S. Yun (San Francisco, CA: ASP), 234
- Hildebrand, R. H., Davidson, J. A., Dotson, J. L., et al. 2000, *PASP*, 112, 1215
- Homan, D. C., Lister, M. L., Aller, H. D., Aller, M. F., & Wardle, J. F. C. 2009, *ApJ*, 696, 328
- Jorstad, S. G., Marscher, A. P., Lister, M. L., et al. 2005, *AJ*, 130, 1418
- Jorstad, S. G., Marscher, A. P., Stevens, J. A., et al. 2007, *AJ*, 134, 799
- Kudryavtseva, N. A., Gabuzda, D. C., Aller, M. F., & Aller, H. D. 2011, *MNRAS*, 415, 1631
- Lee, S.-S., Lobanov, A. P., Krichbaum, T. P, et al. 2008, *AJ*, 136, 159
- Lee, S.-S., Byun, D.-Y., Kim, J., et al. 2011, *PASP*, 123, 1398
- Lee, S.-S., Han, M., Kang, S., et al. 2013, in *European Physical Journal Web of Conf.* 61, *The Innermost Regions of Relativistic Jets and Their Magnetic Fields*, Granada, Spain, ed. J. L. Gómez, 7007
- Lee, S.-S., Petrov, L., Byun, D.-Y., et al. 2014, *AJ*, 147, 77
- Li, H., Dowell, C. D., Kirby, L., Novak, G., & Vaillancourt, J. E. 2008, *Applied Optics*, 47, 422
- Lobanov, A. P. 1998, *A&A*, 330, 79
- Martí-Vidal, I., Muller, S., Vlemmings, W., Horellou, C., & Aalto, S. 2015, *Science*, 348, 311

Plambeck, R. L., Bower, G. C., Rao, R., et al. 2014, *ApJ*, 797,66

Planck Collaboration 2013, *yCat*, 8091, 0

Saikia, D. J. & Salter, C. J. 1988, *ARA&A*, 26, 93

Smith, P. S., Montiel, E., Rightley, S., et al. 2009, in *eConf Proc. C091122* [arXiv:0912.3621], The 2009 Fermi Symposium, Washington

Stevens, J. A., Robson, E. I., & Holland, W. S. 1996, *ApJ*, 462, 23

Tilanus, R. P. J., Krichbaum, T. P., Zensus, J. A., et al. 2014, *ArXiv e-prints*, 1406.4650

Tribble, P. C. 1991, *MNRAS*, 250, 726

Trippe, S., Neri, R., Krips, M., et al. 2010, *A&A*, 515, 40

Trippe, S., Neri, R., Krips, M., et al. 2012, *A&A*, 540, 74

Trippe, S., Bremer, M., Krichbaum, T. P., et al. 2012, *MNRAS*, 425, 1192

Wright, M. C. H., & Forster, J. R. 1980, *ApJ*, 239, 873

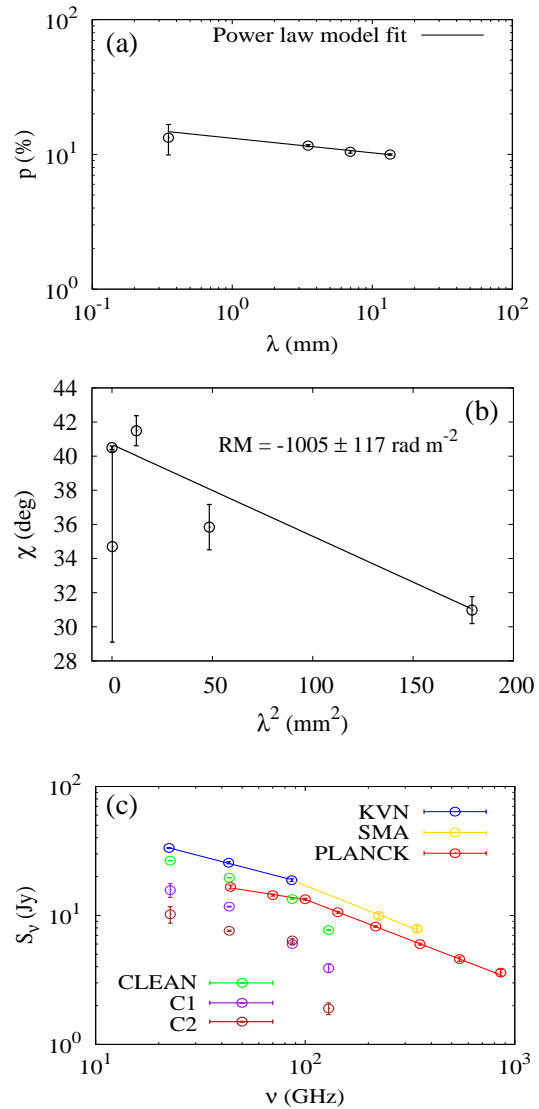


Fig. 2.— (a) Degree of linear polarization of 3C 279 at 13 mm, 7 mm, 3.5 mm, and 350 μm . The solid line is the best fit result of the power law model to the data. (b) EVPAs of 3C 279 at 13 mm, 7 mm, 3.5 mm, 350 μm , and optical. The solid line is the best fit result of the Faraday rotation measure RM to the data. (c) Flux densities of 3C 279 obtained with KVN single dish (blue circles), SMA (yellow circles), PLANCK (red circles), and KVN VLBI observations (green circles for CLEAN images, purple circles for C1 component and brown circles for C2a or C2b component). The solid lines are the best fit results of the spectral index to the data.

This 2-column preprint was prepared with the AAS L^AT_EX macros v5.2.

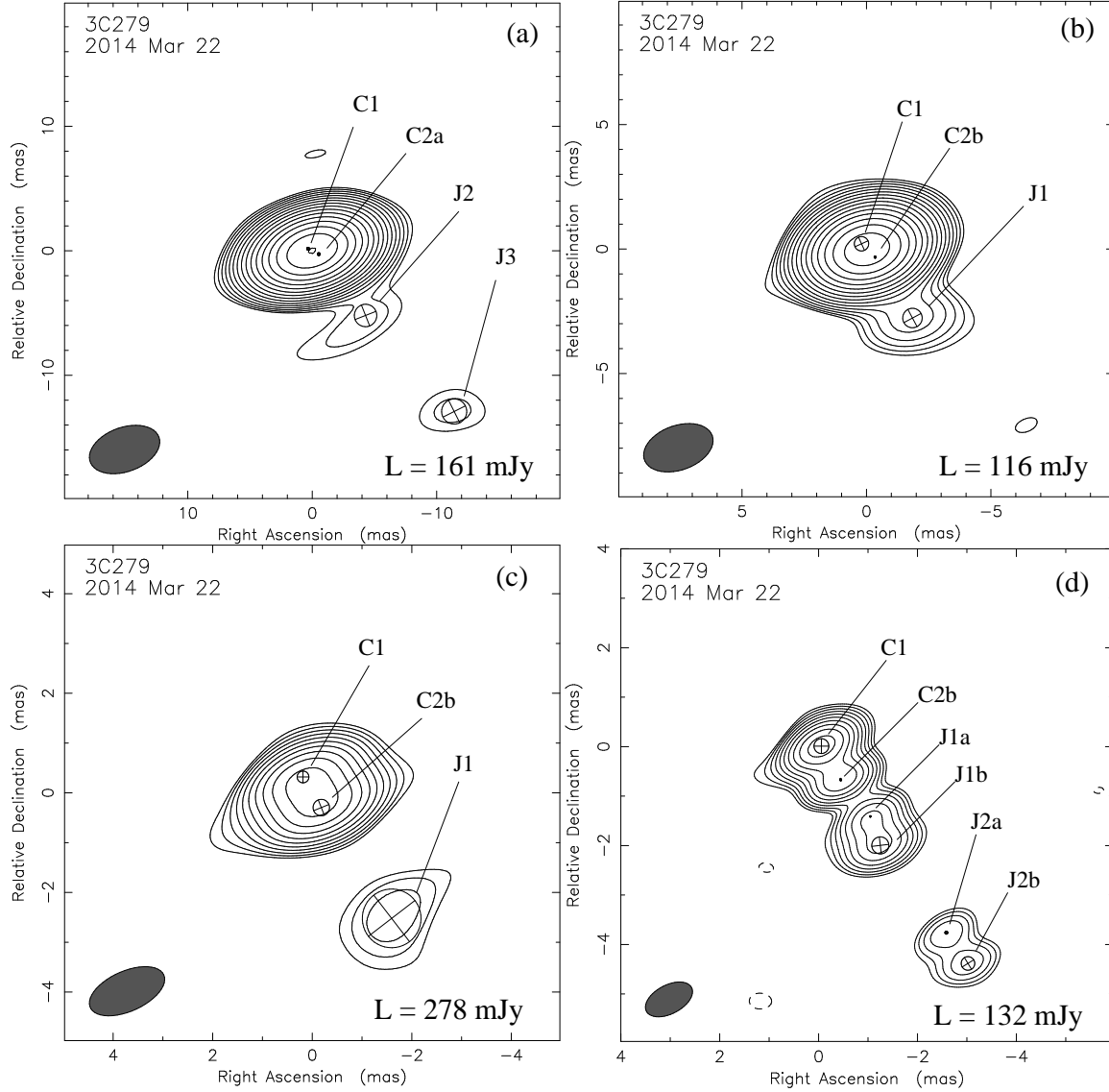


Fig. 3.— CLEANed images of 3C 279 obtained with KVN at (a) 13 mm, (b) 7 mm, (c) 3.5 mm, and (d) 2.3 mm, on 2014 March 22. Circular Gaussian models are on top of the contour map. The axes of each map are the relative R.A. and decl. offsets from the tracking center in mas. The lowest contour level is shown in the lower right corner of each map. The contours have a logarithmic spacing and are drawn at 1, 1.4, ..., 1.4^n of the lowest contour level.